Interaction-Aware Predictive Environmental Control Barrier Function for Emergency Lane Change

Citation for the original published paper (version of record):
Quan, Y., Falcone, P., Sjöberg, J. (2026). Interaction-Aware Predictive Environmental Control Barrier Function for Emergency Lane Change. IEEE Control Systems Letters, 10: 1051-1056.
http://dx.doi.org/10.1109/LCSYS.2026.3704414

(article starts on next page)

Interaction-Aware Predictive Environmental Control Barrier Function for Emergency Lane Change

Ying Shuai Quan, Paolo Falcone, and Jonas Sjöberg, *Member, IEEE*

***Abstract*—Safety-critical motion planning in mixed traffic remains challenging for autonomous vehicles, especially when it involves interactions between the ego vehicle (EV) and surrounding vehicles (SVs). In dense traffic, the feasibility of a lane change depends strongly on how SVs respond to the EV motion. This letter presents an interaction-aware safety framework that incorporates such interactions into a control barrier function (CBF)-based safety assessment. The proposed method predicts near-future vehicle positions over a finite horizon, thereby capturing reactive SV behavior and embedding it into the CBF-based safety constraint. To address uncertainty in the SV response model, a robust extension is developed by treating the model mismatch as a bounded disturbance and incorporating an online uncertainty estimate into the barrier condition. Compared with classical environmental CBF methods that neglect SV reactions, the proposed approach provides a less conservative and more informative safety representation for interactive traffic scenarios, while improving robustness to uncertainty in the modeled SV behavior.**

***Index Terms*—Control barrier function, constrained control, safety-critical control.**

I. Introduction

AUTONOMOUS driving in mixed traffic requires safety-critical decision making in environments where surrounding vehicles (SVs) react to the ego vehicle (EV). This coupling is particularly important in emergency lane changes: when a suddenly appearing road user (RU) blocks the current lane, the feasibility of the maneuver depends not only on the current gap in the target lane, but also on whether the SV yields to the EV. Therefore, safety assessment based only on instantaneous geometry or non-reactive environment models can be overly conservative or even misleading. This is illustrated in Fig. 1, where accounting for the SV reaction opens a feasible gap for lane change, whereas a nominal non-reactive prediction deems the maneuver infeasible.

Received 17 March 2026; revised 25 May 2026; accepted 26 May 2026. Date of publication 17 June 2026; date of current version 30 June 2026. This work was supported by the Fordonsstrategisk Forskning och Innovation Program of Vinnova under Grant 2018-05005. This article has not been presented at a conference. Recommended by Senior Editor R. Vazquez. *(Corresponding author: Ying Shuai Quan.)*

Ying Shuai Quan and Jonas Sjöoberg are with the Mechatronics Group, Department of Electrical Engineering, Chalmers University of Technology, 412 96 Gothenburg, Sweden (e-mail: quany@chalmers.se; jonas.sjoberg@chalmers.se).

Paolo Falcone is with the Mechatronics Group, Department of Electrical Engineering, Chalmers University of Technology, 412 96 Gothenburg, Sweden, and also with the SAAS–Service d'Automatique et Analyse des Systémes, Ecole Polytechnique de Bruxelles, ULB, 1050 Brussels, Belgium (e-mail: paolo.falcone@ulb.be).

Digital Object Identifier 10.1109/LCSYS.2026.3704414

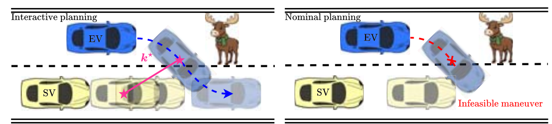

Fig. 1. Interactive versus nominal planning in an obstacle-avoidance lane-change scenario. Faded yellow and blue vehicles indicate predicted future positions of the SV and EV. The blue dotted curve shows interactive planning, where the SV is expected to decelerate and open a feasible gap for lane change. The red dotted curve shows nominal planning, where the SV is assumed to maintain constant velocity, making the maneuver infeasible. The magenta arrow marks $k^\star$, the predicted step with the smallest EV–SV gap, i.e., the "most critical EV–SV configuration".

Control barrier functions (CBFs) have been widely used in autonomous driving for safety-critical control, since they provide forward-invariance guarantees for safe sets while remaining compatible with online optimization-based control synthesis [1], [2]. Environmental CBFs (ECBFs) extend this framework to dynamic environments by reasoning over joint EV–environment dynamics [3]. However, many existing formulations, including ECBFs, still model surrounding traffic as exogenous or non-interactive, which is insufficient for interactive mixed-traffic scenarios.

To capture such interaction in mixed traffic, the SV response must be modeled rather than treated as exogenous. Car-following models provide a natural description of SV longitudinal behavior and can be extended to account for anticipatory reactions to the EV [4]. In practice, however, the true SV behavior is uncertain and may deviate from the nominal model. Such mismatch affects both the magnitude of the SV response and the timing at which the interaction becomes active. A practical interaction-aware safety framework should therefore incorporate both an explicit SV response model and robustness to model uncertainty, while remaining computationally tractable online. Robust CBF formulations [5] address parametric and disturbance uncertainty, but without considering surrounding agents' reactive behavior.

Interaction-aware planning has been extensively studied in MPC [6], game-theoretic [7], and learning-based frameworks [8], but no comparable framework exists within the CBF setting. Motivated by this, we propose an *interaction-aware predictive environmental control barrier function* (IECBF) for emergency lane change. The method incorporates a joint EV–SV model into the ECBF framework, with predictive intelligent driver model (P-IDM) used to capture anticipatory

SV interaction, and constructs a predictive barrier inspired by [9] that evaluates the most critical EV–SV configuration over a finite horizon. To address model uncertainty, we further develop a robust extension that combines observer-based correction for acceleration mismatch with a multi-model rollout for gateway uncertainty. The main contributions of this letter are: 1) We formulate an interaction-aware joint EV–SV model within an ECBF framework and construct a predictive IECBF that evaluates the most critical EV–SV configuration over a finite horizon. 2) We develop a robust extension under SV-model uncertainty by combining observer-based correction for acceleration mismatch with a multi-model rollout for gateway uncertainty. 3) We demonstrate in simulation that compared with a baseline ECBF using a non-reactive SV model, the proposed method empirically improves feasibility and reduces conservatism in interactive emergency lane-change scenarios.

II. Preliminaries

A. Scenario Description

The road is modeled as a straight two-lane segment. We consider an emergency lane-change scenario in which the EV must leave its initial lane due to a suddenly appearing RU and merge into a target lane occupied by a single SV. Throughout the maneuver, the SV is assumed to remain in its lane and react only through longitudinal braking or acceleration.

The objective is to design the EV control input to guarantee collision avoidance while accounting for the SV's reactive behavior through the proposed IECBF framework. CBF constraints enforce safety with respect to both the SV and the suddenly appearing RU, modeled as a temporary static obstacle during lane change, while CLF-based constraints encode the EV's nominal tracking objective.

B. EV Dynamics

We consider continuous-time dynamics. Let $x(t) \in \mathbb{R}^{n_x}$ and $u(t) \in \mathbb{R}^{n_u}$ denote the EV state and control input as:

$$x := \begin{bmatrix} X_e & Y_e & \psi_e & v_e \end{bmatrix}^\top, u := \begin{bmatrix} a_e & \delta_e \end{bmatrix}^\top, \tag{1}$$

where (X_e, Y_e) denotes the position of the EV center of gravity (CG) in the inertial frame, ψ_e is the heading angle, v_e is the longitudinal speed, a_e is the EV longitudinal acceleration and δ_e is the steering angle. The admissible input set is $\mathcal{U} := \{u = [a_e, \delta_e]^\top \in \mathbb{R}^2 : a_e \in [a_{e,\min}, a_{e,\max}],\ \delta_e \in [\delta_{e,\min}, \delta_{e,\max}]\}$. Under a small-angle assumption, the EV dynamics is written as

$$\dot{x} = f(x) + g(x)u, \tag{2}$$

with

$$f(x) = \begin{bmatrix} v_e \cos\psi_e \\ v_e \sin\psi_e \\ 0 \\ 0 \end{bmatrix}, g(x) = \begin{bmatrix} 0 & -v_e \sin\psi_e \\ 0 & v_e \cos\psi_e \\ 0 & \dfrac{v_e}{\ell_r} \\ 1 & 0 \end{bmatrix},$$

where ℓ_r is the distance from the vehicle CG to the rear axle.

C. CLF Design for Lane Change

We employ standard control Lyapunov function (CLF) constraints to encode the nominal lane-change objective [1]. Let Y_{target} denote the center line of the target lane. During the lane-change maneuver, it serves as the reference for the EV lateral position and heading. We define $V_y(x) := \big(Y_e - Y_{\text{target}}\big)^2$, $V_\psi(x) := \psi_e^2$ where V_y penalizes lateral deviation from the target-lane center, while V_ψ penalizes heading deviation from the road direction. Here, for a continuously differentiable scalar function V, the Lie derivatives of V along f and g are defined as $L_f V(x) := \nabla V(x)^\top f(x)$ and $L_g V(x) := \nabla V(x)^\top g(x)$. The corresponding CLF constraints are imposed as soft constraints in a quadratic programming (QP) problem:

$$L_f V_\ell(x) + L_g V_\ell(x)\, u \le -\alpha_\ell\big(V_\ell(x)\big) + \delta_\ell, \ell \in \{y, \psi\}, \tag{3}$$

where α_ℓ are class-$\mathcal{K}$ functions and $\delta_\ell \ge 0$ are slack variables. These soft constraints promote lateral tracking and heading regulation whenever compatible with safety.

D. Baseline ECBF Formulation

This subsection presents a baseline ECBF design for the lane-change scenario using an EV–SV joint-state representation equivalent to the augmented-state form in [3], with the SV modeled as non-reactive at constant velocity.

1) Baseline Joint EV–SV Model: Let the SV state be $x_s := \begin{bmatrix} X_s & Y_s & v_s \end{bmatrix}^\top$, where (X_s, Y_s) denotes the position of the SV CG in the inertial frame, and v_s denotes its longitudinal speed. The joint EV–SV state is then defined as

$$z := \begin{bmatrix} x^\top & x_s^\top \end{bmatrix}^\top. \tag{4}$$

With SV's nominal dynamics given by $\dot{x}_s = \bar{f}_s(x_s)$, $\bar{f}_s(x_s) := \begin{bmatrix} v_s \\ \mathbf{0}_{2\times 1} \end{bmatrix}$ and combining with (2), the nominal joint dynamics are

$$\dot{z} = \bar{F}(z) + \bar{G}(z)u, \bar{F}(z) := \begin{bmatrix} f(x) \\ \bar{f}_s(x_s) \end{bmatrix}, \bar{G}(z) := \begin{bmatrix} g(x) \\ \mathbf{0}_{3\times 2} \end{bmatrix}. \tag{5}$$

2) ECBF Design: For the baseline joint system (5), define the safe set $\mathcal{C}_z := \{z \in \mathcal{Z} : H(z) \ge 0\}$, where $H : \mathcal{Z} \to \mathbb{R}$ is continuously differentiable.

Definition 1: [ECBF]

A continuously differentiable function $H : \mathcal{Z} \to \mathbb{R}$ is called an ECBF for (5) if there exists a class-$\mathcal{K}$ function α_H such that, for all $z \in \mathcal{C}_z$,

$$\sup_{u\in\mathcal{U}} \big(L_F H(z) + L_G H(z)\, u\big) \ge -\alpha_H\big(H(z)\big). \tag{6}$$

If a locally Lipschitz controller $u : \mathcal{C}_z \to \mathcal{U}$ satisfies

$$L_F H(z) + L_G H(z)\, u(z) \ge -\alpha_H\big(H(z)\big), \quad \forall z \in \mathcal{C}_z, \tag{7}$$

then $\mathcal{C}_z$ is forward invariant [3].

To enforce collision avoidance between the EV and the SV, we choose $H_{\text{SV}}(z)$ based on the relative EV–SV position expressed in the EV body frame, let $\begin{bmatrix} \Delta X \\ \Delta Y \end{bmatrix} = R(\psi_e)^\top \begin{bmatrix} X_s - X_e \\ Y_s - Y_e \end{bmatrix}$ with $R(\psi_e) = \begin{bmatrix} \cos\psi_e & -\sin\psi_e \\ \sin\psi_e & \cos\psi_e \end{bmatrix}$. Here, ΔX and ΔY denote the longitudinal and lateral gaps in the EV body frame, respectively. We then define the ECBF candidate as

$$H_{\text{SV}}(z) = a_{\text{SV}}\Delta X^2 + b_{\text{SV}}\Delta Y^2 - 1, \tag{8}$$

where $a_{\text{SV}} = 1/(r_a^{\text{SV}})^2$ and $b_{\text{SV}} = 1/(r_b^{\text{SV}})^2$, with r_a^{SV} and r_b^{SV} denoting the longitudinal and lateral semi-axes of the ellipsoidal safety envelope. Then with α_{SV} as a class-$\mathcal{K}$ function, the baseline ECBF constraint is

$$L_{\bar{F}} H_{\text{SV}}(z) + L_{\bar{G}} H_{\text{SV}}(z)\, u \ge -\alpha_{\text{SV}}\big(H_{\text{SV}}(z)\big). \tag{9}$$

E. RU ECBF

The suddenly appearing RU is modeled as a static obstacle at fixed position $(X_{\mathrm{RU}}, Y_{\mathrm{RU}})$ over the short emergency lane change, which is a special case of the ECBF framework with constant environment state. We define the RU barrier as

$$H_{\mathrm{RU}}(x) := a_{\mathrm{RU}}(X_e - X_{\mathrm{RU}})^2 + b_{\mathrm{RU}}(Y_e - Y_{\mathrm{RU}})^2 - 1, \tag{10}$$

where $a_{\mathrm{RU}} = 1/(r_a^{\mathrm{RU}})^2$ and $b_{\mathrm{RU}} = 1/(r_b^{\mathrm{RU}})^2$. Since the RU position is constant, H_{RU} depends only on the EV state, and its Lie derivatives are taken with respect to the EV dynamics (2). The corresponding ECBF constraint is

$$L_f H_{\mathrm{RU}}(x) + L_g H_{\mathrm{RU}}(x)\, u \ge -\alpha_{\mathrm{RU}}\big(H_{\mathrm{RU}}(x)\big). \tag{11}$$

where α_{RU} is a class-$\mathcal{K}$ function. Since a_e does not appear in (11), the constraint is affine only in δ_e and reduces to

$$[L_g H_{\mathrm{RU}}(x)]_2\, \delta_e \ge -\alpha_{\mathrm{RU}}\big(H_{\mathrm{RU}}(x)\big) - L_f H_{\mathrm{RU}}(x). \tag{12}$$

III. Interaction-Aware ECBF Design

A. SV Dynamics via P-IDM

The proposed method models SV dynamics based on the P-IDM car-following model in [4]. Unlike standard intelligent driver model (IDM), which assigns the leader based on the candidate vehicle's current lateral position and thus reacts only after lane intrusion, P-IDM uses the predicted lateral position at a short horizon N_{p} ahead. This better captures anticipatory SV behavior in lane-change scenarios, where the candidate vehicle is the EV.

To encode this leader-selection logic compactly, we introduce the gate variable

$$\omega := \begin{cases} 1, & \text{if } X_e > X_s \text{ and } \left|\tilde{Y}_{e,N_{\mathrm{p}}} - Y_s\right| < c, \\ 0, & \text{otherwise}, \end{cases} \tag{13}$$

where c is a cooperation threshold that determines the SV's willingness to yield. Thus, $\omega = 1$ means that the EV is treated as the SV's leader based on its predicted lane intrusion. In the lane-change scenarios considered here, ω transitions from 0 to 1 at most once and remains at 1 thereafter. When the EV is selected as leader, the SV longitudinal acceleration is computed using the standard IDM [10],

$$a_{\mathrm{idm}} := a_{\max}\left[1 - \left(\frac{v_s}{v^*}\right)^4 - \left(\frac{s^*(v_s, \Delta v_s)}{\Delta x_s}\right)^2\right], \tag{14}$$

where v^* is the desired speed, $a_{\max}$ is the maximum acceleration, $\Delta x_s = X_e - X_s$ is the bumper-to-bumper gap between the EV and the SV, and $\Delta v_s = v_s - v_e$ is the relative approach speed. The desired minimum gap is given by $s^*(v_s, \Delta v_s) = s_0 + v_s T_{\mathrm{idm}} + \frac{v_s \Delta v_s}{2\sqrt{a_{\max} b}}$, where s_0 is the standstill distance, T_{idm} is the desired time headway, and b is the comfortable deceleration. $a_{\mathrm{free}} := a_{\max}\left[1 - \left(\frac{v_s}{v^*}\right)^4\right]$. Then the resulting P-IDM acceleration can be written as

$$a_{\mathrm{pidm}} := \omega\, a_{\mathrm{idm}}(\Delta x_s,\, v_s,\, \Delta v_s) + (1 - \omega)\, a_{\mathrm{free}}(v_s). \tag{15}$$

Accordingly, the SV dynamics in the proposed model are

$$\dot{x}_s = f_s(x, x_s), \qquad f_s(x, x_s) := \begin{bmatrix} v_s \\ 0 \\ a_{\mathrm{pidm}} \end{bmatrix}, \tag{16}$$

where the dependence on the EV state enters through a_{pidm}.

B. Interaction-Aware Joint EV–SV Model

To explicitly capture the interaction between the EV and SV, we combine (2) with (16). With the joint state (4), the interaction-aware joint dynamics take the control-affine form

$$\dot{z} = F(z) + G(z)u, \tag{17}$$

where $F(z) := \begin{bmatrix} f(x) \\ f_s(x, x_s) \end{bmatrix}, G(z) := \begin{bmatrix} g(x) \\ \mathbf{0}_{3\times 2} \end{bmatrix}$. Here, $F(z)$ represents the natural evolution of the combined EV–SV state, including the SV response, and $G(z)$ specifies how the EV input u enters the joint dynamics.

C. IECBF Constraints for SV

In the proposed method, safety assessment is extended over a short prediction horizon under the interaction-aware SV response, since interaction effects may not be immediately visible but emerge as the SV reacts to the EV. Accordingly, we use two ECBF constraints: a current-position ECBF for present-state safety and a predictive ECBF over the finite horizon under the interaction-aware joint model.

1) One-Step IECBF: We use the same SV barrier function $H_{\mathrm{SV}}^{\mathrm{curr}}(z) = H_{\mathrm{SV}}(z)$ as in the baseline ECBF (8). From here on, we write $H_{\mathrm{SV}}^{\mathrm{curr}} := H_{\mathrm{SV}}^{\mathrm{curr}}(z)$ for brevity. The one-step ECBF constraint under the joint dynamics (17) is then

$$L_F H_{\mathrm{SV}}^{\mathrm{curr}} + L_G H_{\mathrm{SV}}^{\mathrm{curr}}\, u \ge -\alpha_{\mathrm{SV}}\big(H_{\mathrm{SV}}^{\mathrm{curr}}\big). \tag{18}$$

Compared with the baseline (9), the term $L_F H_{\mathrm{SV}}^{\mathrm{curr}}$ now reflects the interaction-aware SV dynamics through a_{pidm}.

2) Predictive ECBF: To explicitly account for near-future interaction, we construct a predictive barrier by rolling out the joint model (17) over a finite horizon N.

a: Nominal rollout controller: To roll out (17), we use a nominal steering controller that drives the EV toward the target lane while satisfying the RU ECBF constraint (11). The SV barrier is not enforced in the rollout, since SV safety is handled by the outer predictive ECBF and enforcing it in the inner rollout would bias the predicted trajectory.

By (12), the RU ECBF together with the steering bounds yields the feasible interval $\delta_e \in [\delta_{\min}^{\mathrm{RU}}, \delta_{\max}^{\mathrm{RU}}]$. Within this interval, the nominal steering is chosen from the 1-D soft CLF–CBF problem

$$\min_{\delta_e \in [\delta_{\min}^{\mathrm{RU}}, \delta_{\max}^{\mathrm{RU}}]} \quad H_\delta\, \delta_e^2 + p_y \max(0, \phi_y)^2 + p_\psi \max(0, \phi_\psi)^2,$$

where $\phi_y := L_f V_y + [L_g V_y]_2\, \delta_e + \alpha_y(V_y), \phi_\psi := L_f V_\psi + [L_g V_\psi]_2\, \delta_e + \alpha_\psi(V_\psi)$, following the standard soft-constraint CLF–CBF construction of [1]. Since this is a scalar soft CLF–CBF problem, its minimizer admits a closed-form solution [2], so no online optimization is required in the rollout. Denoting the resulting steering command at prediction step k by $\delta_{e,k}^{\mathrm{nom}}$, the nominal rollout input is

$$u_k^{\mathrm{nom}} := \begin{bmatrix} 0 & \delta_{e,k}^{\mathrm{nom}} \end{bmatrix}^\top. \tag{19}$$

The nominal rollout sets $a_e = 0$ because the CLF and RU ECBF terms used here determine only the steering input δ_e; a_e is neither constrained nor optimized in the inner rollout.

b: Predictive barrier and constraint: Let $\{z_k\}_{k=0}^N$ denote the rollout from the current state z_0, where the EV is propagated using (2) under the nominal control (19) over a horizon N. At each rollout step, we evaluate $H_{\mathrm{SV}}(z_k)$. The most critical predicted step is

$$k^* = \arg \min_{k \in \{0, \ldots, N\}} H_{\mathrm{SV}}(z_k). \tag{20}$$

If multiple k attain the minimum, the smallest is selected. We then define the predictive barrier as

$$H_{\mathrm{SV}}^{\mathrm{pred}}(z_0) := H_{\mathrm{SV}}(z_{k^*}), \tag{21}$$

i.e., the minimum predicted barrier value along the rollout. Let $J_{k^*} := \partial z_{k^*}/\partial z_0$ denote the rollout Jacobian from the current state to the critical predicted state. Then

$$\begin{aligned} L_F H_{\mathrm{SV}}^{\mathrm{pred}}(z_0) &= \nabla_z H_{\mathrm{SV}}(z_{k^*})\, J_{k^*}\, F(z_0), \\ L_G H_{\mathrm{SV}}^{\mathrm{pred}}(z_0) &= \nabla_z H_{\mathrm{SV}}(z_{k^*})\, J_{k^*}\, G(z_0). \end{aligned} \tag{22}$$

Using the same class-$\mathcal{K}$ function α_{SV} as in (18), and writing $H_{\mathrm{SV}}^{\mathrm{pred}} := H_{\mathrm{SV}}^{\mathrm{pred}}(z_0)$ for brevity, the predictive ECBF constraint enforced in the outer QP is

$$L_F H_{\mathrm{SV}}^{\mathrm{pred}} + L_G H_{\mathrm{SV}}^{\mathrm{pred}}\, u \geq -\alpha_{\mathrm{SV}}\big(H_{\mathrm{SV}}^{\mathrm{pred}}\big). \tag{23}$$

Constraint (23) complements the one-step constraint (18): the latter enforces safety at the current state, while the former accounts for the most critical EV–SV configuration over the prediction horizon under the interaction-aware joint model.

D. Nominal CLF-IECBF QP

The nominal CLF–IECBF QP is finally given as

$$u^\star = \arg\min_{\substack{u\in\mathcal{U},\\ \delta_y,\delta_\psi}} \frac{1}{2}u^\top Q u + \frac{1}{2}p_y\delta_y^2 + \frac{1}{2}p_\psi\delta_\psi^2 \quad \text{s.t.} \;\; (3),\ (11),\ (18),\ (23). \tag{24}$$

Like most CLF–CBF QPs, (24) provides no formal feasibility guarantee, though the interaction-aware rollout empirically reduces SV barrier conservatism, improving feasibility over the baseline (Section V).

IV. Robust IECBF Under IDM Model Uncertainty

The IECBF in Section III uses a nominal P-IDM model for SV prediction. In practice, the true SV behavior may deviate due to uncertain driver characteristics. This mismatch appears in both the SV acceleration magnitude after interaction becomes active and the timing of interaction gate activation. To address both, this section extends the IECBF with observer-based correction for acceleration mismatch and a multi-model rollout for gateway uncertainty.

A. Uncertainty Modeling

1) IDM Parameter Uncertainty: Let $\theta := (a_{\max}, v^*, s_0, T_{\mathrm{idm}}, b)$ denote the IDM parameter vector. For later use in the multi-model rollout, let $j \in \mathcal{J}$ index a finite set of representative IDM parameter presets, with each j associated with an IDM parameter vector $\theta^{(j)}$. Let θ_{nom} denote the preset nominal parameter set. Let θ^* denote the unknown true IDM parameter vector. Then the true SV longitudinal acceleration is modeled as

$$\dot{v}_s = a_{\mathrm{idm}}(\theta_{\mathrm{nom}}) + \Delta_\theta, \tag{25}$$

where $\Delta_\theta := a_{\mathrm{idm}}(\theta^*) - a_{\mathrm{idm}}(\theta_{\mathrm{nom}})$. Accordingly, the interaction-aware joint dynamics (17) are rewritten as

$$\dot{z} = F(z) + G(z)u + B_s\,\Delta_\theta, \tag{26}$$

where $B_s := \begin{bmatrix}0\ 0\ 0\ 0\ 0\ 0\ 1\end{bmatrix}^\top$.

We assume that the uncertainty and its rate of change are bounded:

$$|\Delta_\theta| \leq \delta_b, \qquad |\dot{\Delta}_\theta| \leq \delta_L, \tag{27}$$

for known constants $\delta_b, \delta_L > 0$, determined offline from the admissible range of SV driver behavior.

The sensitivity of the predictive barrier to the acceleration perturbation $B_s\Delta_\theta$ at the current state is defined as $\sigma := \nabla_z H_{\mathrm{SV}}(z_{k^*})\, J_{k^*}\, B_s = [\nabla_z H_{\mathrm{SV}}(z_{k^*})\, J_{k^*}]_{v_s}$, i.e., the v_s-component of the propagated gradient. σ quantifies how the current SV acceleration perturbation affects the barrier at the critical step k^*, and is used below in the robust predictive IECBF constraint.

2) Gateway Activation Uncertainty: To capture gateway activation uncertainty, we consider a finite set of representative P-IDM gateway parameter pairs $\varphi^{(i)} = (N^{(i)}, c_{\mathrm{th}}^{(i)})$, $i \in \mathcal{I}$. Since gate activation depends on both the gateway preset and the IDM model used in the rollout, we denote the corresponding interaction gate for model pair (i, j) by $\omega^{(i,j)}$, where $i \in \mathcal{I}$ and $j \in \mathcal{J}$. Hence, even for the same $\varphi^{(i)}$, different IDM presets $\theta^{(j)}$ can yield different gate activations and switching times between free-road and car-following behavior along the predicted trajectory. This uncertainty is relevant only when $\omega^{(i,j)} = 1$, i.e., when the SV is predicted to react to the EV through the IDM car-following model under $(\varphi^{(i)}, \theta^{(j)})$. When $\omega^{(i,j)} = 0$, the SV follows the free-road model $a_{\mathrm{free}}(\theta^{(j)})$, so the car-following mismatch Δ_θ is inactive. Accordingly, the robust correction for IDM parameter uncertainty is applied only while the corresponding gate $\omega^{(i,j)}$ is active.

B. Gate-Activated Car-Following Observer

Following [5], we estimate the SV car-following acceleration mismatch online from the measured SV speed v_s, only when the corresponding interaction gate is active, i.e., $\omega^{(i,j)} = 1$. Define the uncertainty estimate as $\hat{\Delta}_\theta := \lambda_s v_s - \xi$, where $\xi \in \mathbb{R}$ is the observer state and $\lambda_s > 0$ is the observer gain. During intervals with $\omega^{(i,j)} = 1$, the observer dynamics are

$$\dot{\xi} = \lambda_s\big(a_{\mathrm{idm}}(\theta^{(j)}) + \hat{\Delta}_\theta\big). \tag{28}$$

At each $0 \to 1$ transition of $\omega^{(i,j)}$, the observer state is reset according to $\xi \leftarrow \lambda_s v_s$ so that $\hat{\Delta}_\theta = 0$ at the reset instant.

Let $t_{\mathrm{cf}} \geq 0$ denote the elapsed time since the most recent observer-gate activation, and define the estimation error as

$$e_\theta := \Delta_\theta - \hat{\Delta}_\theta. \tag{29}$$

Lemma 1: Suppose the uncertainty Δ_θ satisfies (27). Then, along each interval with $\omega^{(i,j)} = 1$, the estimation error e_θ satisfies $\dot{e}_\theta = \dot{\Delta}_\theta - \lambda_s e_\theta$, and is bounded by

$$|e_\theta(t)| \leq \bar{e}(t_{\mathrm{cf}}) := \left(\delta_b - \frac{\delta_L}{\lambda_s}\right) e^{-\lambda_s t_{\mathrm{cf}}} + \frac{\delta_L}{\lambda_s}, \tag{30}$$

for all $t_{\mathrm{cf}} \geq 0$.

Proof: The result follows directly from Lemma 1 in [5]. □

Thus, the bound resets to δ_b at each $0 \to 1$ transition of $\omega^{(i,j)}$ and then decays monotonically to δ_L/λ_s during the corresponding interaction-active interval. Define $t_{\mathrm{conv}} := 2/\lambda_s$, i.e., two time constants after gate activation. Since the exponential term in (30) is then reduced to $e^{-2} \approx 13.5\%$ of its initial value, t_{conv} is used as a conservative proxy for observer convergence, and $\hat{\Delta}_\theta$ is treated as reliable only when $t_{\mathrm{cf}} > t_{\mathrm{conv}}$.

C. Robust Predictive ECBF Constraint

1) Case-Dependent Predictive Rollout: The overall uncertainty set is the Cartesian product $\mathcal{M} := \mathcal{I} \times \mathcal{J}$, where each model $m = (i, j) \in \mathcal{M}$ defines one complete SV driver description by combining one gateway preset and one IDM kinematic preset. Prediction is then organized by $\omega^{(i,j)}$, $t_{\mathrm{cf}} \geq 0$, and a braking detection condition evaluated once the observer has converged. Specifically, let

$$\mathcal{B}^{(i,j)} := \left\{ a_{\mathrm{idm}}(\theta^{(j)}) + \hat{\Delta}_\theta \ < \ a_{\mathrm{free}}(\theta^{(j)}) - \varepsilon \right\}, \tag{31}$$

denote the event that, under the model pair (i, j), the observer-corrected SV acceleration falls below the corresponding free-flow prediction by a margin $\varepsilon > 0$, indicating that the SV has begun car-following deceleration. Based on $\omega^{(i,j)}$, t_{cf}, and $\mathcal{B}^{(i,j)}$, three mutually exclusive cases are considered.

a: Case 1: $\omega^{(i,j)} = 0$ for all $(i, j) \in \mathcal{M}$: No interaction gate is active under any model pair, so the SV remains in free-flow for all $(i, j) \in \mathcal{M}$. The observer is inactive, and no online correction is available.

b) Case 2: $\omega^{(i,j)} = 1$ for at least one $(i, j) \in \mathcal{M}$ and $t_{cf} \leq t_{conv}$: At least one gate is active and the observer is running, but $\hat{\Delta}_\theta$ is still transient and not yet reliable.

c) Case 3: $\omega^{(i,j)} = 1$ for at least one $(i, j) \in \mathcal{M}$, $t_{cf} > t_{conv}$, and $\mathcal{B}^{(i,j)}$ holds: The observer has converged and the corrected prediction confirms active SV deceleration for the corresponding model pair (i, j). Only in this case does prediction switch from the multi-model evaluation over $\mathcal{M}$ to a single observer-corrected rollout for the active model pair, with correction $\hat{\Delta}_\theta$ injected.

If $\omega^{(i,j)} = 1$ for at least one $(i, j) \in \mathcal{M}$ and $t_{\mathrm{cf}} > t_{\mathrm{conv}}$ but $\mathcal{B}^{(i,j)}$ does not hold, then the observer has converged but the SV still remains in free-flow under the active model pair. The situation therefore reduces to Case 1. The observer continues running, and the system switches to Case 3 once $\mathcal{B}^{(i,j)}$ is satisfied.

2) Multi-Model Rollout for Cases 1 and 2: In Cases 1 and 2, all $|\mathcal{M}|$ models are rolled out from the current state z_0. For each $m = (i, j) \in \mathcal{M}$, N forward steps are simulated using the joint dynamics f, with the SV acceleration at step k given by $a_{\mathrm{sv},k}^{(m)} = a_{\mathrm{pidm}}\big(\theta^{(j)}\big)$. No observer correction is injected. The worst-case evaluation point is selected over all trajectories and prediction steps:

$$(m^*, k^*) \ := \ \arg \min_{\substack{m \in \mathcal{M}, \\ k \in \{1, \ldots, N\}}} H_{\mathrm{SV}}\big(z_k^{(m)}\big). \tag{32}$$

$J_{k^*} = \mathrm{d}z_{k^*}/\mathrm{d}z_0$ is then propagated through the winning trajectory $\{z_k^{(m^*)}\}$ using the parameter set of m^*.

3) Observer-Corrected Rollout for Case 3: In Case 3, the observer has converged and SV braking is confirmed for a model pair (i, j) via $\mathcal{B}^{(i,j)}$ in (31). A single rollout is then performed for that pair, with observer correction injected:

$$a_{\mathrm{sv},k}^{(i,j)} = a_{\mathrm{pidm}}\big(\theta^{(j)}, \varphi^{(i)}\big) + \hat{\Delta}_\theta \, \omega_k^{(i,j)}. \tag{33}$$

The critical step k^* is selected via (20), and the Jacobian in (22) is propagated along the resulting corrected trajectory.

4) Robust Predictive and Current-Position IECBF Constraints: This subsection applies only to Case 3. In this case, both the predictive barrier and its current-position special case are evaluated from the observer-corrected rollout in (33).

a: Predictive IECBF: Under the perturbed joint dynamics (26), the time derivative of $H_{\mathrm{SV}}^{\mathrm{pred}}$ along the true trajectory satisfies $\dot{H}_{\mathrm{SV}}^{\mathrm{pred}} = L_F H_{\mathrm{SV}}^{\mathrm{pred}} + L_G H_{\mathrm{SV}}^{\mathrm{pred}} u + \sigma \Delta_\theta \geq \widetilde{L}_F H_{\mathrm{SV}}^{\mathrm{pred}} + L_G H_{\mathrm{SV}}^{\mathrm{pred}} u$, where $\tau := |\sigma| \, \bar{e}(t_{\mathrm{cf}})$ and $\widetilde{L}_F H_{\mathrm{SV}}^{\mathrm{pred}} := L_F H_{\mathrm{SV}}^{\mathrm{pred}} + \sigma \hat{\Delta}_\theta$. Accordingly, the robust predictive IECBF constraint for Case 3 is

$$\widetilde{L}_F H_{\mathrm{SV}}^{\mathrm{pred}} + L_G H_{\mathrm{SV}}^{\mathrm{pred}} u - \tau \geq -\alpha_{\mathrm{SV}}\big(H_{\mathrm{SV}}^{\mathrm{pred}}\big). \tag{34}$$

TABLE I
P-IDM PRESETS

IDM preset	$a_{\max}$ [m/s^2]	b [m/s^2]	Gateway preset	N_p	c [m]
Conservative	2.0	3.0	Cautious	10	1.0
Normal	4.0	5.0	Normal	20	2.0
Aggressive	6.0	6.0	Cooperative	40	3.0

All presets share $s_0 = 10\,\mathrm{m}$, $T_{\mathrm{idm}} = 1.5\,\mathrm{s}$, and $v^* = 10\,\mathrm{m/s}$.

b: Current-position guard: The current-position guard is the $N = 0$ special case of the predictive barrier, i.e., $H_{\mathrm{SV}}^{\mathrm{curr}} = H_{\mathrm{SV}}(z_0)$. Accordingly, define $\sigma_0 := \frac{\partial H_{\mathrm{SV}}^{\mathrm{curr}}}{\partial v_s}(z_0)$, $\tau_0 := |\sigma_0| \, \bar{e}(t_{\mathrm{cf}})$ and $\widetilde{L}_F H_{\mathrm{SV}}^{\mathrm{curr}} := L_F H_{\mathrm{SV}}^{\mathrm{curr}} + \sigma_0 \hat{\Delta}_\theta$, then the robust current-position guard for Case 3 is

$$\widetilde{L}_F H_{\mathrm{SV}}^{\mathrm{curr}} + L_G H_{\mathrm{SV}}^{\mathrm{curr}} u - \tau_0 \geq -\alpha_{\mathrm{SV}}\big(H_{\mathrm{SV}}^{\mathrm{curr}}\big). \tag{35}$$

Theorem 1 (Robust current-position safety in Case 3): Consider Case 3. Suppose the true SV acceleration satisfies (25) and (27), and let $\hat{\Delta}_\theta$ and $\bar{e}(t_{\mathrm{cf}})$ be generated as in Section IV-B. If u is locally Lipschitz and satisfies (35) for all $t \geq 0$, then the set $\mathcal{C}_{\mathrm{SV}}^{\mathrm{curr}} = \{z \in \mathcal{Z} \mid H_{\mathrm{SV}}^{\mathrm{curr}}(z) \geq 0\}$ is forward invariant. Hence, if $H_{\mathrm{SV}}^{\mathrm{curr}}(z(0)) \geq 0$ at $t = 0$, then $H_{\mathrm{SV}}^{\mathrm{curr}}(z(t)) \geq 0$ for all $t \geq 0$.

Proof: By (35), $\dot{H}_{\mathrm{SV}}^{\mathrm{curr}}(z) \geq -\alpha_{\mathrm{SV}}\big(H_{\mathrm{SV}}^{\mathrm{curr}}(z)\big)$. Since α_{SV} is class-$\mathcal{K}$, the standard CBF comparison argument yields forward invariance of $\mathcal{C}_{\mathrm{SV}}^{\mathrm{curr}}$ [5]. □

The predictive constraint (34) is anticipatory, accounting for the most critical predicted EV–SV configuration over the horizon. Unlike the current-position guard (35), it does not yield forward invariance, since $H_{\mathrm{SV}}^{\mathrm{pred}}$ is nonsmooth at switching instants of $k^\star$. Instead, (34) steers the QP away from configurations flagged as critical. The rollout's $a_e = 0$ assumption likewise affects only $H_{\mathrm{SV}}^{\mathrm{pred}}$, not the forward-invariance guarantee of Theorem 1.

D. Robust CLF–IECBF QP

For $\ell \in \{\mathrm{pred}, \mathrm{curr}\}$, define

$$\widehat{L}_F H_{\mathrm{SV}}^{\ell} := \begin{cases} L_F H_{\mathrm{SV}}^{\ell}, & \text{Cases 1-2}, \\ \widetilde{L}_F H_{\mathrm{SV}}^{\ell} - \tau_\ell, & \text{Case 3}, \end{cases}$$

with $\tau_{\mathrm{pred}} = \tau$ and $\tau_{\mathrm{curr}} = \tau_0$. The robust CLF–IECBF QP is finally given as

$$\begin{aligned} u^\star = \ & \arg \min_{\substack{u \in \mathcal{U}, \\ \delta_y, \delta_\psi}} \frac{1}{2} u^\top Q u + \frac{1}{2} p_y \delta_y^2 + \frac{1}{2} p_\psi \delta_\psi^2 \\ & \text{s.t.} \ \ (3), \ (11), \\ & \quad \widehat{L}_F H_{\mathrm{SV}}^{\ell} + L_G H_{\mathrm{SV}}^{\ell} u \geq -\alpha_{\mathrm{SV}}\big(H_{\mathrm{SV}}^{\ell}\big), \ell \in \{\mathrm{pred}, \mathrm{curr}\}. \end{aligned} \tag{36}$$

V. SIMULATION RESULTS

The proposed framework is built on top of `highway-env` [11]. All simulations were run on a MacBook Pro equipped with an Apple M3 chip.[1] The simulation is set up as described in Section II-A. The representative P-IDM settings are shown in Table I and the remaining design parameters are shown in Table II. During the simulation, the true SV behavior is generated by a *conservative* IDM model with a *cautious* gateway, whereas the EV nominal joint model assumes an *aggressive* SV IDM model with a *cooperative* gateway. The EV is initialized in the upper lane at $(X_e(0), Y_e(0)) = (20, \ \ Y_{\mathrm{upper}})$,

[1]Supplementary video: https://www.youtube.com/watch?v=01j8KXr36tU

TABLE II
SIMULATION, CONTROLLER, AND ROBUST-DESIGN PARAMETERS

Parameter	Value	Parameter	Value	Parameter	Value
$v_e(0)$	10 m/s	p_y	25	λ_s	$10\,\mathrm{s}^{-1}$
$v_s(0)$	12.5 m/s	p_ψ	15	δ_b, δ_L	$0.5\,\mathrm{m/s}^2$
$r_a^{\mathrm{RU}}, r_b^{\mathrm{RU}}$	2.0 m	κ_y, κ_ψ	1.5	κ_{SV}	5
r_a^{SV}	4.5 m	$a_{e,\max}$	$5\,\mathrm{m/s}^2$	$\delta_{e,\min}$	-1.8 rad
r_b^{SV}	2.5 m	$a_{e,\min}$	$-5\,\mathrm{m/s}^2$	$\delta_{e,\max}$	$+1.8$ rad

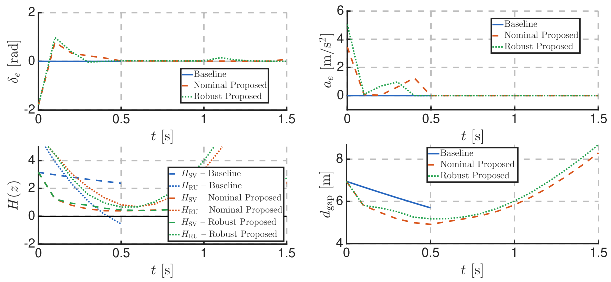

Fig. 2. EV control inputs δ_e and a_e, CBF values and d_{gap} generated by the baseline, nominal proposed, and robust proposed controllers.

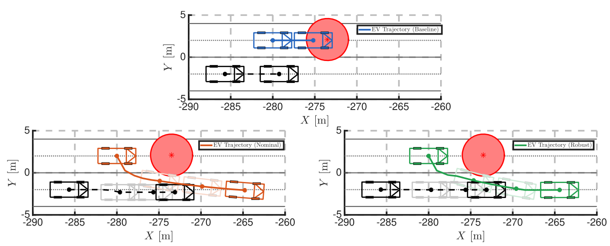

Fig. 3. Global trajectories for the baseline, nominal proposed, and robust proposed controllers. In all three plots, the SV is the black vehicle in the lower lane and the red ellipse denotes the RU CBF level set $\{H_{\mathrm{RU}} = 0\}$.

and the SV is initialized in the lower lane at $(X_s(0), Y_s(0)) = (X_e(0) - 5.5,\ Y_{\text{lower}})$. The RU is placed in the upper lane at $(X_{\mathrm{RU}}, Y_{\mathrm{RU}}) = (X_e(0)+6,\ Y_{\text{upper}})$. The simulation sampling time is $\Delta t = 0.1$ s. Here, Y_{upper} and Y_{lower} denote the lateral positions of the centers of the upper and lower lanes, respectively. Linear class-$\mathcal{K}$ functions are used for both the CLF and CBF constraints: $\alpha_{\mathrm{RU}}(s) = \kappa_{\mathrm{RU}} s, \alpha_{\mathrm{SV}}(s) = \kappa_{\mathrm{SV}} s, \alpha_y(s) = \kappa_y s, \alpha_\psi(s) = \kappa_\psi s$, where $\kappa_{\mathrm{SV}} > 0$, $\kappa_{\mathrm{RU}} > 0$, $\kappa_y > 0$, and $\kappa_\psi > 0$ are design parameters. $N = 20$ is chosen to balance coverage of the SV reaction window against rollout cost. $\delta_{e,\max}$ and $\delta_{e,\min}$ are set permissively to accommodate aggressive steering in the emergency lane-change context. Baseline, nominal and robust proposed controllers are compared in the simulation. For a fair comparison, the baseline controller also adopts the predictive CBF structure, including both the current and the predictive SV safety constraint together with the RU CBF constraint. The difference is that its predictive rollout is based on the baseline non-interactive model (5).

Figure 2 compares the baseline, nominal proposed, and robust proposed controllers. The baseline controller becomes infeasible immediately. As a result, both the steering and acceleration inputs remain zero, the EV cannot initiate an effective avoidance maneuver, and the vehicle continues toward the RU. This is further confirmed by the RU barrier value H_{RU} which drops below zero at around 0.4 s, indicating loss of safety. The corresponding global trajectory in Figure 3 shows that the EV eventually collides with the RU obstacle. In contrast, both the nominal proposed and robust proposed controllers remain feasible throughout the maneuver and generate feasible control actions from solving the QP, as shown in Figure 2. The inner-vehicle distance $d_{\text{gap}}(t) := \sqrt{(X_e - X_s)^2 + (Y_e - Y_s)^2}$ is also compared in Fig. 2. The difference between the nominal proposed and robust proposed controllers is more clearly seen in the global trajectories in Figure 3. For the nominal proposed controller, the internal joint model assumes a more cooperative SV response than the true one. Because of this model mismatch, although the EV completes the maneuver safely and the barrier values remain nonnegative, the true SV exhibits a small lateral deviation, visible in its trajectory. This deviation is generated by the built-in background-vehicle behavior in `highway-env`, where SVs follow IDM longitudinal dynamics together with a MOBIL-based lateral policy [11]. By contrast, the robust proposed controller accounts for this mismatch through the multi-model predictive rollout and observer-based tightening, and therefore avoids this undesirable lateral displacement of the SV while still maintaining feasibility and safety. Figure 2 shows that the nominal proposed and robust proposed controllers keep the barrier values nonnegative throughout the maneuver, whereas the baseline controller violates the RU safety constraint. These results show that the proposed interaction-aware predictive CBF empirically improves feasibility relative to the baseline model, and that the robust extension further improves the physical consistency of the interaction.

VI. CONCLUSION

This letter proposed an IECBF for emergency lane change in mixed traffic, incorporating an interaction-aware joint EV–SV model with P-IDM into the ECBF framework. As demonstrated in simulation, compared with classical ECBF neglecting SV reactions, the proposed method empirically improves feasibility and safety. A robust extension combining multi-model rollout with observer-based correction addresses SV-model uncertainty, further improving feasibility under model mismatch. The framework extends to multiple lanes, RUs, and SVs by replicating per-agent constraints. Lateral SV maneuvers are left for future work.

REFERENCES

[1] A. D. Ames, X. Xu, J. W. Grizzle, and P. Tabuada, "CBF-based quadratic programs for safety-critical systems," *IEEE Trans. Autom. Control*, vol. 62, no. 8, pp. 3861–3876, Aug. 2017.

[2] M. Jankovic, "Robust CBFs for constrained stabilization of nonlinear systems," *Automatica*, vol. 96, pp. 359–367, Oct. 2018.

[3] T. G. Molnar, A. K. Kiss, A. D. Ames, and G. Orosz, "Safety-critical control with input delay in dynamic environments," *IEEE Trans. Control Syst. Technol.*, vol. 31, no. 4, pp. 1507–1520, Jul. 2023.

[4] B. Brito, A. Agarwal, and J. Alonso-Mora, "Learning interaction-aware guidance for trajectory optimization," *IEEE Trans. Intell. Transp. Syst.*, vol. 23, no. 10, pp. 18808–18821, Oct. 2022.

[5] E. Daş and J. W. Burdick, "Robust control barrier functions using uncertainty estimation with application to mobile robots," *IEEE Trans. Autom. Control*, vol. 70, no. 7, pp. 4766–4773, Jul. 2025.

[6] Y. Chen, U. Rosolia, W. Ubellacker, N. Csomay-Shanklin, and A. D. Ames, "Interactive motion planning with branch MPC," *IEEE Robot. Automat. Soc.*, vol. 7, no. 2, pp. 5365–5372, Apr. 2022.

[7] Z. Huang, H. Liu, and C. Lv, "Interactive multi-modal motion planning with branch model predictive control," *IEEE Robot. Automat. Lett.*, Oct. 2023, pp. 3903–3913.

[8] Y. Hu et al., "Planning-oriented autonomous driving," in *Proc. CVPR*, Jun. 2023, pp. 17853–17862.

[9] J. Breeden and D. Panagou, "Predictive CBFs for online safety-critical control," in *Proc. 61st IEEE Conf. Decis. Control (CDC)*, Cancun, Mexico, Dec. 2022, pp. 924–931.

[10] M. Treiber, A. Hennecke, and D. Helbing, "Congested traffic states in empirical observations," *Phys. Rev. E, Stat. Phys. Plasmas Fluids Relat. Interdiscip. Top.*, vol. 62, no. 2, p. 1805, 2000.

[11] E. Leurent. (2018). *An Environment for Autonomous Driving Decision-Making*. [Online]. Available: https://github.com/eleurent/highway-env